Journal of Alloys and Compounds 823 (2020) 153733

Contents lists available at ScienceDirect

Journal of Alloys and Compounds

journal homepage: http://www.elsevier.com/locate/jalcom

An investigation on the properties of boron modified Cu–Al–Be polycrystalline shape memory alloys

Guniputi Bala Narasimha , S.M. Murigendrappa *

Department of Mechanical Engineering, National Institute of Technology Karnataka, Surathkal, 575025, India

ARTICLE INFO

Article history:
Received 20 August 2019
Received in revised form
4 January 2020
Accepted 6 January 2020
Available online 11 January 2020

Keywords:
Cu–Al-Be shape memory alloy
Boron
Aluminium diboride (AlB_2)
Heterogeneous nucleation
Grain refinement
Serrated grains

ABSTRACT

Effect of microalloying of boron (B) i.e., 0.02–0.15 wt% and the variation of composition of Al and Be from 11.3 to 11.9 wt% and 0.41–0.44 wt% respectively, has been investigated on the grain refinement and shape memory properties of polycrystalline Cu–Al–Be shape memory alloy. The tests have been carried out for microstructure, morphology, phases, crystal structure, phase transformation temperatures and shape recovery ratio. The investigation results in boron has strong impact on grain refinement with minimal addition, followed by Al and Be. AlB_2 acts as heterogeneous nucleation site in grain refinement and it increases with increase in B and Al. Transformation temperatures increases with boron up to 0.08 wt% and then decreases, whereas increase in Al and Be decreases the temperatures. Doping and increasing of boron up to 0.15 wt% exhibits complete shape recovery, whereas Be < 0.42 wt% and Al < 11.8 wt% exhibits poor recovery ratio.

1. Introduction

Among family of shape memory alloys (SMA), Cu–Al-X (X = Be, Mn, Ni and Zn) shape memory alloys captivates researchers to develop, investigate and analyse various methods to overcome the key limitations i.e., brittleness [1,2], martensite stabilization [3,4], thermal stability [5,6] and shape memory detoriation for the practical applications. Cu–Al are chosen as an alternative to other SMAs because of economical and ease of production. Among the family of Cu–Al-X alloys, Cu–Al–Be SMAs exhibits lower/intermediate transformation temperatures, high pseudo elasticity and better damping capacity suitable for civil and space structure applications, but restricted in real time because of intergranular failure (poor ductility) and short life (functional fatigue) related to coarse grain size and high elastic anisotropy.

It is learned from the existing literature, that grain size can be tailored by various factors viz. elemental composition [7], inoculation using grain refiners [8], heat treatment [9] and quenching media [10], and novel processing routes viz. powder metallurgy [11], rapid solidification [12] and ECAP [13]. Inoculation by Boron (B), Chromium (Cr), Zirconium (Zr) [14,15], rare earths (RRE) [16–18] and their composition has high influence on the grain size, growth rate for the bulk alloys compared to other factors and routes. It is also understood that varying elemental composition of the matrix and inoculants not only refines the grains, also does modification of phases, increases/decreases transformation tempeartures [19] affects martensitic transformation. Boron attracts attention in grain refinement and plays as an effective grain refiner for Cu [20], Mg [21], Al [22], Cu-Al [23] systems because of its advantages like small atomic radius i.e., which acts as an either substitutional or interstitial solid solution element, and de-embrittle element which enhances the cohesive strength of grain boundaries [24] and moreover, very small lattice disregistry. Boron combines with other metals to form metal borides such as AlB_2, TiB_2 and ZrB_2 forms nucleation sites in enhancing grain refinement.

Cu–Al alloys can be effectively grain refined with minimal addition i.e., 0.02–0.05 wt% of B with improved mechanical properties [25] due to the lower lattice disregistry. Lee [26] investigated the addition of various borides to Cu–Zn–Al SMA and noticed good grain refinement with the AlB_2 compared to other. Dong [27,28] studied shape memory capacity and life of Cu–Al– Be alloy with addition of 0.02 wt% of B, and noticed complete restoration, and there is no discussion on grain size refinement and mechanism. Sampath [29,30] and Aydogdu [31] observed good refinement with decrease in SME and SE, with the addition of B to Cu–Al–Mn alloys. Ping Zhang [13] studied the effect of 0.18 wt% of B in grain

* Corresponding author.
E-mail addresses: balanarasimha.g@gmail.com (G. Bala Narasimha), smm@nitk.ac.in (S.M. Murigendrappa).

https://doi.org/10.1016/j.jallcom.2020.153733
0925-8388/

refinement of Cu–Al–Be alloy under Equal Channel Angular pressing (ECAP) route, noticed that reduction in grain size of 2 μm with uniform distribution of precipitated phases after 8 passes. The shape recovery ratio of fine-grained Cu–Al–Be–B SMA was not better than that of the as-cast alloy. Sampath [32] didn't noticed martensitic transformation with the addition of 0.2 wt% of B, due to the formation of bulky precipitates inhibits the formation of martensite variants. Sutou [33,34] observed addition of B increases the damping efficiency of Cu–Al–Mn alloys.

Based on literature survey, it is understood that addition of boron more than 0.15 wt% leads to poor shape recovery and also reveals dearth of experimentation on effect of variation in the composition of elements on properties of Cu–Al–Be–B alloys. This drives us to investigate the effect of variation in wt% of alloying elements and microalloying of boron i.e., 0.02 to 0.15 wt% on grain refinement, phases, transformation tempeartures and shape recovery properties.

2. Materials and methods

2.1. Alloy and specimen preparation

In the present work, high purity i.e., >99.9% of Copper (Cu), Aluminium (Al), Beryllium (Be) and Boron (B) was used for the preparation of alloys. Initially, an inoculant viz. copper-boron (CuB_2) master alloy was prepared using vacuum arc remelting machine (Make: Edmund Buhler GmbH, Model: AM/0.5) and cut into small pieces as shown in Fig. 1, and the composition (EDS) is shown in Fig. 2.

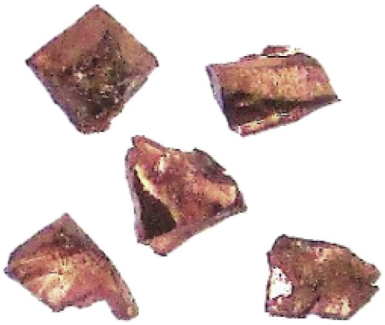

Fig. 1. Photograph of CuB_2 inoculant.

Table 1 presents the variations of elemental composition of Cu, Al, Be, B in wt.%., and the alloys are designated as "B_{XY}", 'X' represents the type of alloy, 'Y' represents the wt.% of boron. Y = 1,2,3,4,5,6 for 0.02, 0.04,0.06,0.08,0.1 and 0.15 wt% of B, respectively. Alloys were prepared using an induction melting furnace under inert gas atmosphere. Casted alloys were heat treated in muffle furnace at 850 °C for 4 h under argon gas atmosphere for homogeneous mixture without oxidation, and then cooled to room temperature. After homogenization, alloys were hot rolled at 800 °C into a sheet of 0.5 mm thickness with intermediate annealing for shape recovery studies. Alloy samples for microstructural, XRD and shape recovery studies were betatized at 850 °C for 15 min and then directly quenched into water (RT) and hold for 10 min.

2.2. Characterization

Samples were polished and etched using FeCl3 solution for microstructure and morphology studies using optical microscope (Make: Zeiss, Model: Axiolab A1) and scanning electron microscope (SEM, Make: JEOL, Model: JSM-6380LA) respectively, and the elemental composition of the matrix and precipitates were determined using energy-dispersive X-ray spectroscopy (EDS, Make: EDAX, Model: Element). Average grain size of the alloys were calculated using ASTM E 1382- semiautomatic and automatic image analysis. XRD tests were performed on samples using X-ray diffractometer (Make: Rigaku, Model: Miniflex 600) at room temperature under CuKα1 radiation (λ = 1.54056 A°), 40 kV and 15 mA from 2θ = 20°–90° at a scan rate of 2°/min. for the identification of phases exist and its crystal structure. Phase transformation temperatures of the quenched alloys were measured using power compensated differential scanning calorimeter (DSC, Make: PerkinElmer, Model: 6000) with heating and cooling rate of 10°/min. Shape recovery ratio (SRR) of the alloys were measured by the bend test as illustrated in Fig. 3. The test procedure is as follows, the sheet at full martensite state ($\leq M_f$) was bent around a mandrel and unloaded viz. from A-A to A-B, this angle measured as θ_d. The deformed sheet was heated above 10 °C of the austenite finish temperature, and it tends to attain the original position with or without residual strain, i.e., A-C or A-A, respectively, this angle

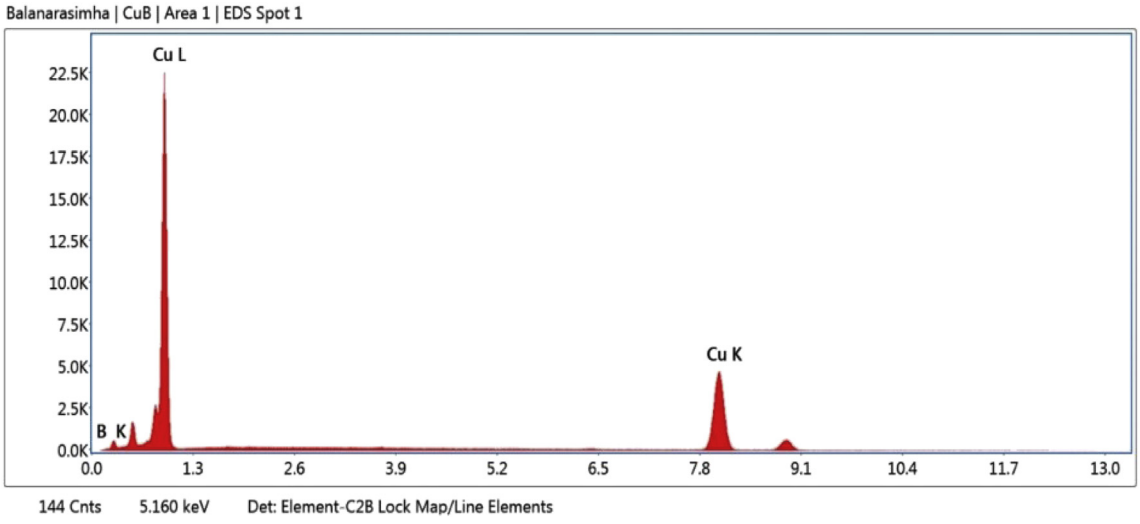

Fig. 2. Energy dispersive spectrum (EDS) of CuB_2.

Table 1
Elemental composition of Cu, Al, Be, B shape memory alloys.

S. No	Alloy	Actual Composition (wt.%)			B (wt.%)
		Cu	Al	Be	
Al, Be — constant, Boron - Increase					
1.	B_{11}	87.64	11.90	0.44	0.02
2.	B_{12}	87.62	11.90	0.44	0.04
3.	B_{13}	87.6	11.90	0.44	0.06
4.	B_{14}	87.58	11.90	0.44	0.08
5.	B_{15}	87.56	11.90	0.44	0.10
6.	B_{16}	87.51	11.90	0.44	0.15
Be, B — constant, Aluminium - Increase					
7.	B_{21}	87.67	11.90	0.41	0.02
8.	B_{31}	87.57	12.00	0.41	0.02
9.	B_{44}	87.89	11.60	0.45	0.08
10.	B_{54}	87.57	11.90	0.45	0.08
Al, B — constant, Beryllium - Increase					
11.	B_{62}	88.17	11.37	0.42	0.04
12.	B_{72}	88.19	11.36	0.43	0.04
13.	B_{21}	87.68	11.90	0.41	0.02
14.	B_{11}	87.64	11.90	0.44	0.02

measured as θ_r.

The shape recovery ratio computed using Eq. (1) [18].

$$\eta = \frac{\theta_d - \theta_r}{\theta_d} \quad (1)$$

where θ_d - angle after deformation and θ_r - residual angle after recovery.

3. Results and discussion

3.1. XRD — phase identification

Inoculation/varying elemental composition in the alloy causes modification of grain size and formation of new phases. Thus, it is necessary to investigate the mechanism behind the process. XRD was employed to study the existence of phases in the alloys, and the results are presented in Figs. 4–7. Red, blue, orange, green, black and pink colored lines represent boron addition of 0.02, 0.04, 0.06, 0.08, 0.1 and 0.15 wt%, respectively. Diffractograms reveals various phases present in the alloys, and refinement of grain size confirmed from their intensities, peak positions and FWHM.

Fig. 4 presents diffractogram of B_{1Y} alloys. Diffractogram conveys that betatized and quenched alloys are of complete martensite phase of $\beta_1^{'}$ (Cu_3Al) and $\gamma^{'}$ ($Cu_{6.11}Al_{3.89}$), along with secondary phases of AlB_2 and $AlB_{25}Cu_{0.79}$. Secondary phases i.e., AlB_2 and $AlB_{25}Cu_{0.79}$ are of rich in boron and aluminium composition, and the mechanism of formation of these phases are discussed in deatiled in the section 3.2. The phases $\beta_1^{'}$, $\gamma^{'}$, AlB_2, $AlB_{25}Cu_{0.79}$ has of monoclinic (M18R), rhombohedral, rhombohedral and tetragonal structures, confirmed and indexed using ICDD 00-028-0005, 00-019-0010, 03-065-3381 and 01-077-2461 respectively. B_{1Y} series indicates refinement of grain size with increase in boron confirms from the decrease in intensities and increase in FWHM of the peaks of M18R (P-3,4,6) and AlB_2 (P-11). It is also observed that the intensity of $\gamma^{'}$ martensite (P-9) increases with the increase in addition of B.

Diffractograms of B_{21} and B_{31} (Fig. 5) discerns that the quenched alloys are in a state of martensite along with a new phase "α_2" (P-10), confirmed and indexed using ICDD 00-028-0006. Phase "α_2" is of Cu_4Al composition with cubic structure, forms around the temperature between 350 and 200 °C [35], quenched from high temperature β (Cu_3Al) phase of the alloy. In this case, though the alloys are rich in aluminium and rapidly quenched from 850 °C to water at RT (30 °C), phase "α_2" formation may be due to the very low addition of Be i.e., 0.41 wt%, affects the cooling rate in the formation of martensite. It is also observed increase in 0.1 wt% Al from B_{21} to B_{31}, affects the martensite fraction confirm from their intensities of peaks.

Diffractogram of B_{44} and B_{54} depicted in Fig. 6, discerns that the alloy B_{54} possess and exhibits additional two phases (peak 8, 12) viz. $Al_{3.89}Cu_{6.11}$ and $AlB_{25}Cu_{0.9}$ are of $\gamma^{'}$ rhombohedral martensite and boron rich secondary phase, compared to B_{44}. The existence of two phases attributed to increase in 0.3 wt% of Al forms the mixture of two variants of martensites $\beta_1^{'} + \gamma^{'}$ [35,36] and the affinity towards B forms boron rich $AlB_{25}Cu_{0.9}$ phase.

Diffractogram B_{62} and B_{72} (Fig. 7) reveals martensite M18R and AlB_2, without $AlB_{25}Cu_{0.9}$ and $Al_{3.89}Cu_{6.11}$ phases due to the very low addition of B (0.02) and the minimum addition of Al compared to former alloys.

From the diffractograms of all the alloys, the salient observations are: a) Addition of B to the matrix forms AlB_2 precipitates and along with increase in Al forms $AlB_{25}Cu_{0.9}$ phases i.e., rich in in boron and

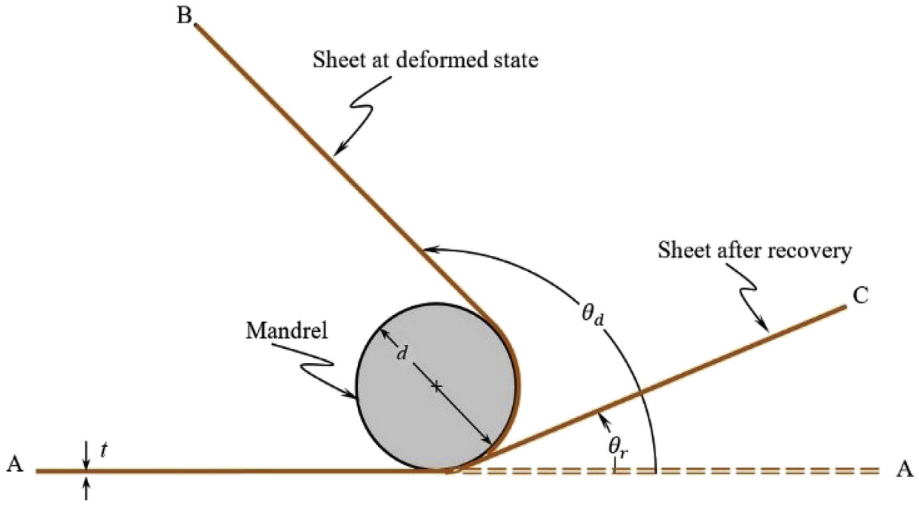

Fig. 3. Bend test.

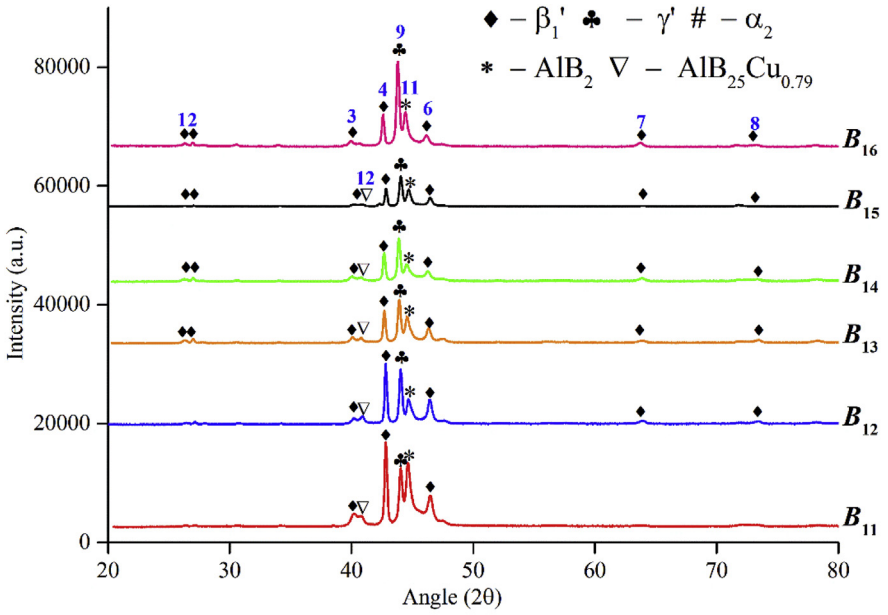

♦ β_1' - 1 (111), 2 (0 1 11), 3 (2 0 2), 4 (0 0 22), 5 (12 10), 6 (20 12), 7 (0 3 17) , 8 (2 1 28)
♣ γ' - 9 (3 0 6) , # α_2 . 10 (2 2 1) * **AlB_2** - 11 (1 0 1), ∇ $AlB_{25}Cu_{0.79}$ - 12 (2 0 2)

Fig. 4. X-ray diffractograms of B_{1Y} alloys.

aluminium. b) Increase in Al and Be increases the martensite fraction. c) Addition of Be < 0.42 wt% forms phase "α_2" d) Micro alloying of boron confined only to grain refinement, without any phase formation/modification like Al and Be. e) The prime martensite peak of all the alloys are (0 0 18) except in the series B_{21} and B_{31} (1 2 10), i.e., due to the lower addition of Be i.e.< 0.42 wt%. f) γ' martensite ($Al_{3.89}Cu_{6.11}$) and Al–B rich phase ($AlB_{25}Cu_{0.9}$) forms only above 11.8 wt% of Al, has higher affinity towards B forms these phases/precipitates attributes to the difference in electronegativity.

3.2. Microstructure and morphology

Varying elemental composition/heat treatment of alloys affects the grain size and it is confirmed from the micrographs of the betatized and quenched alloys as shown in Figs. 8–9 Microstructures of the quenched alloys exhibits complete lath martensite at room temperature in the form of needles, and the grains were refined to various sizes for the variation in the elemental composition. It is worth noting to be observed that the grain boundaries of

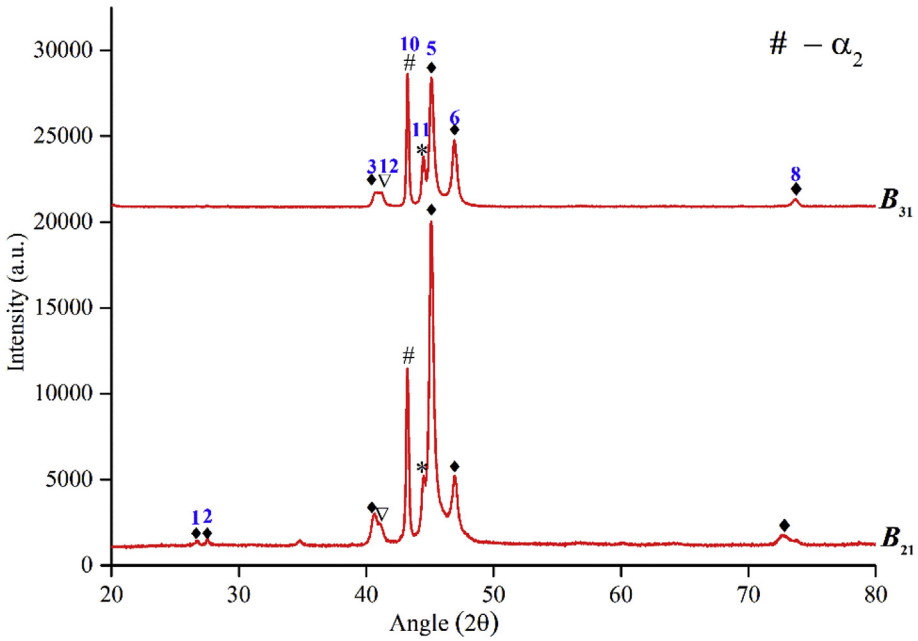

Fig. 5. X-ray diffractograms of B_{21} and B_{31} alloys.

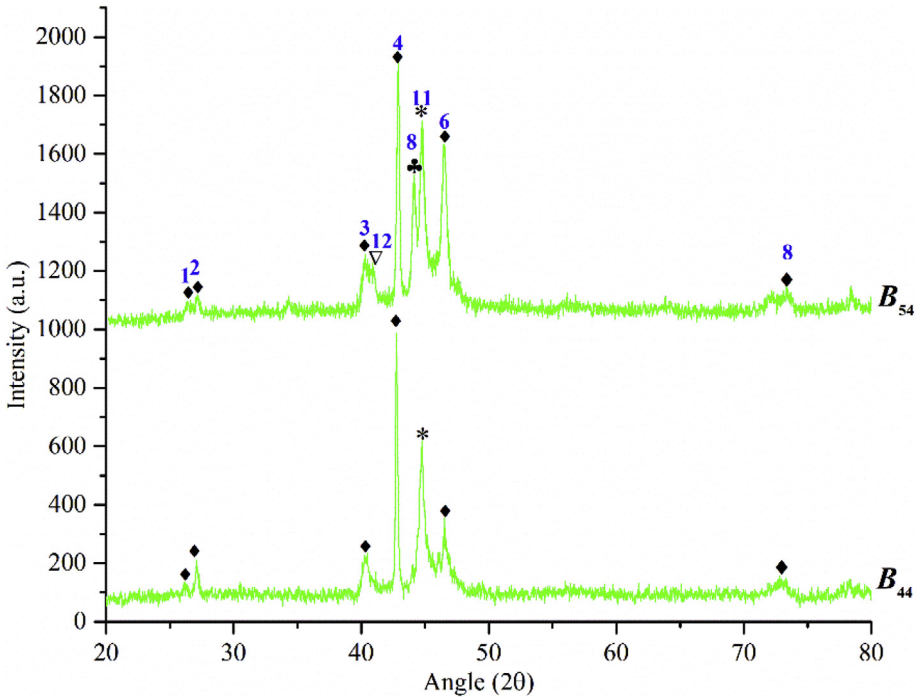

Fig. 6. X-ray diffractograms of B_{44} and B_{54} alloys.

alloys are highly non-uniform/serrated and confirmed with the existing literature [8,26,37,38]. Average grain size was calculated using ASTM E −1382 by taking an average of 20 horizontal and 20 vertical line measurements, because of the irregularity in the grains.

Fig. 8 depicts the microstructures of B_{1Y} alloys, and observed increase in boron exhibits improved refinement in grain size to 134.7, 89.03, 73.33, 68.58, 51.64 and 40.19 μm for B_{11}, B_{12}, B_{13}, B_{14}, B_{15} and B_{16} respectively, with minimal addition of B.

Grain refinement mechanisms are as follows:

i. *Heterogeneous nucleation* – Based on XRD results, it is observed that addition of B to the alloy forms fine AlB_2 (aluminium diboride) phase/precipitates and dissolves in the solid solution [26] confirmed from the SEM-EDS. AlB_2 forms due to the boron is a surface-active element and tends to

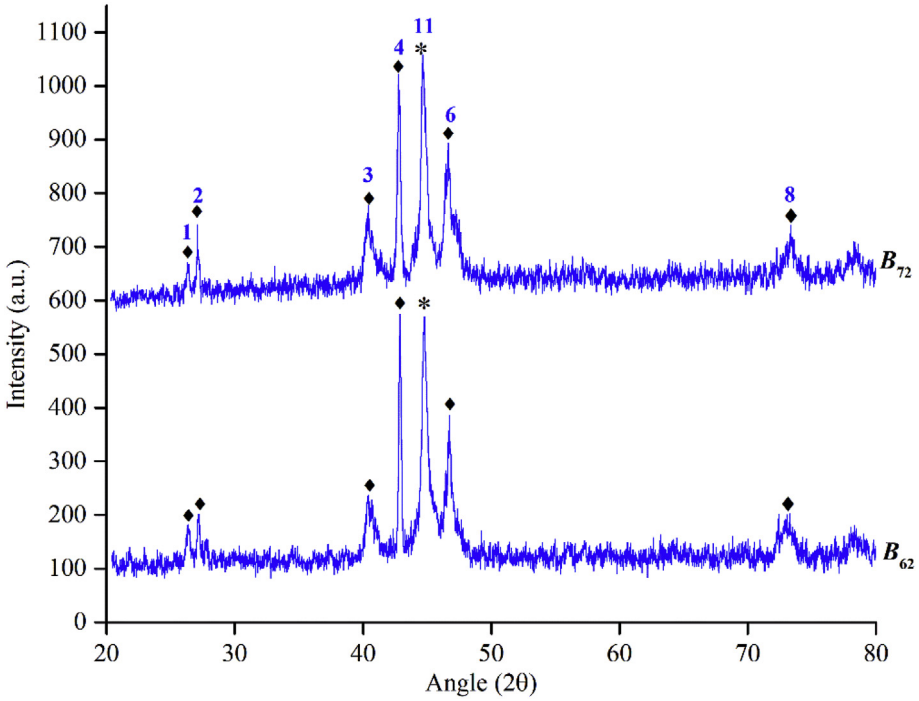

Fig. 7. X-ray diffractograms of B_{62} and B_{72} alloys.

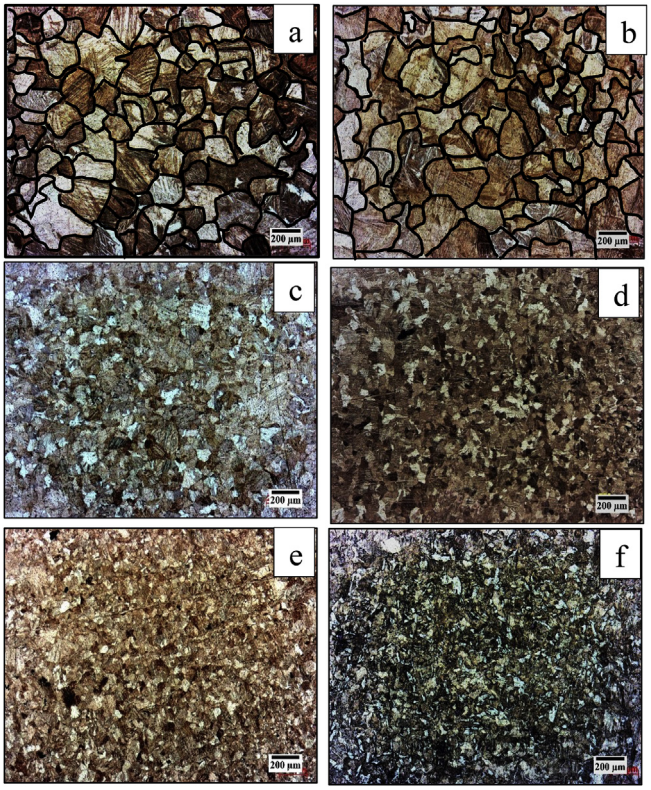

Fig. 8. Microstructures of alloys; (a) B_{11} (b) B_{12}, (c) B_{13}, (d) B_{14}, (e) B_{15} and (f) B_{16} – 50×

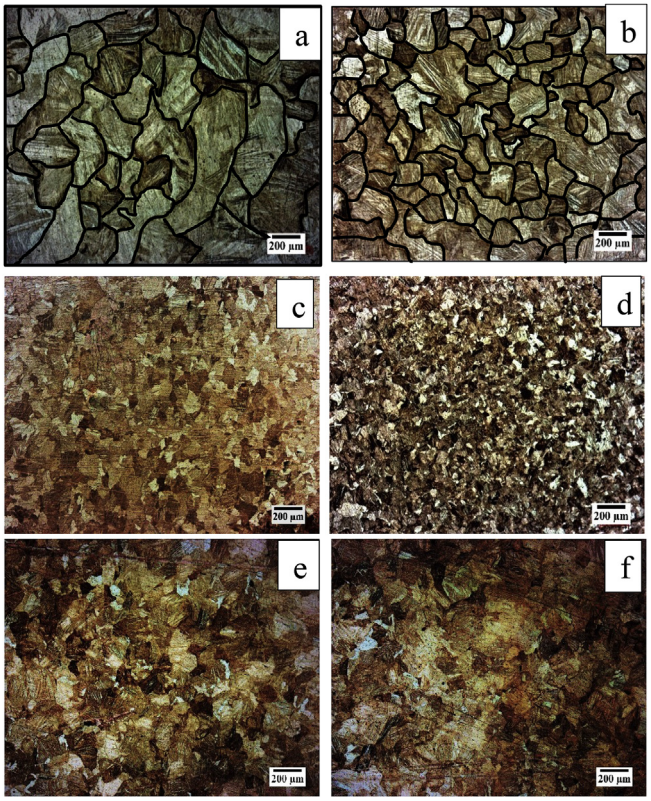

Fig. 9. Microstructures of alloys; (a) B_{21} (b) B_{31}, (c) B_{44}, (d) B_{54}, (e) B_{62} and (f) B_{72} – 50×

diffuse throughout the matrix at the high temperature and segregates at the grain boundaries [20] after quenching to room temperature due to its low solubility and very small atomic radius. In Cu, B has solubility of 0.01 wt% [39] and in Al it has no solubility forms Al + AlB_2 intermetallic particles by a peritectic reaction [40,41] at room temperature. These AlB_2 particles/precipitates, acts as nucleant in refinement of grains [21,23]. It is also observed from SEM-EDS studies, that the accumulation of increased density of AlB_2 particles at the grain interfaces, inhibits the grain growth.

ii. *Growth Restriction factor (GRF)* - It is observed, that B has strong impact on grain refinement with minimal addition as shown in Fig. 8, due to its highest growth restriction factor (GRF) in Cu [24] and Al [22,42] systems, followed by Be in Cu [24]. High GRF (Q) in the alloy is due to the increase in constitutional undercooling increases the driving force for the nucleation at the solid/liquid interface, because of rejection of B in the grains and accumulates at the boundary.

iii. *Lattice disregistry*: difference in the lattice misfit (disregistry) was very small percentage, i.e., 12.59% and 33.0% between the matrix and the nucleant viz. "Cu_3Al – B″ and "Cu_3Al – AlB_2", respectively.

It is also important to present the factors for the formation of serrated boundaries, i.e., these are formed due to the non-homogeneous deposition of boron at the grain boundaries forms increase density of borides "AlB_2" at the interfaces of grains causes lattice distortion [43] and strain differences [44]. Serrated grains are observed in the Mg alloy systems doped with boron [45].

Fig. 9a–d depicts the microstructure of B_{21}, B_{31}, B_{44} and B_{54} alloys, i.e., increase in Al and maintaining other elements constant. It is observed that the reduction in grain size from B_{21} to B_{31} and B_{44} to B_{54} is 210.27 µm–139.85 µm and 81.84 µm–36.97 µm, respectively. Improved grain refinement in both the series of alloys are due to the increase in concentration of AlB_2 particles creates more nucleation sites, and it is confirmed from the diffractograms (Figs. 5 and 6), i.e., increase in intensity of AlB_2 (P-11) of B_{31} and B_{54} compared to B_{21} and B_{44}. Fig. 9e and f depicts the microstructure of alloys with increase in Be and maintaining other elements constant, and observed a reduction in grain size from 144.74 to 128.71 in B_{62} and B_{72} alloys, and from 210.27 to 134.7 in B_{21} and B_{11} alloys (Figs. 9a and 8a), respectively. It is observed that increase in 0.1% of Be doesn't affect the grain size much and confirmed from XRD (Fig. 7), whereas 0.3 wt% of Be exhibits improved refinement as reported in the literature [46,47].

Morphology of grains, grain boundaries and the elemental composition of the phases are captured using SEM-EDS as shown in Fig. 10. Secondary electron images of B doped alloys reveals the grain boundaries are serrated as discussed in the microstructure. It is to be noticed that the B is in lower concentration in the centre of the grain and it increases towards grain boundaries as shown in the EDS spectrum of the alloys Figs (10a-d), due to the seggregation of B while quenching as discussed in the grain refinement mechanism. The distribution of Cu, Al and B in the alloy are captured using elemental mapping as shown in Fig. 10e.

3.3. Phase transformation temperatures

Phase transformation temperatures of the prepared alloys are useful in design and development of an actuator for application in the requisite temperature. DSC was employed to determine transformation tempeartures and the energy (enthalpies) required for phase transformations as discussed in Section 2., and the recorded DSC thermograms are presented with colored lines to differentiate the wt.% of B and its effect on tempeartures as shown in Figs. 11–14.

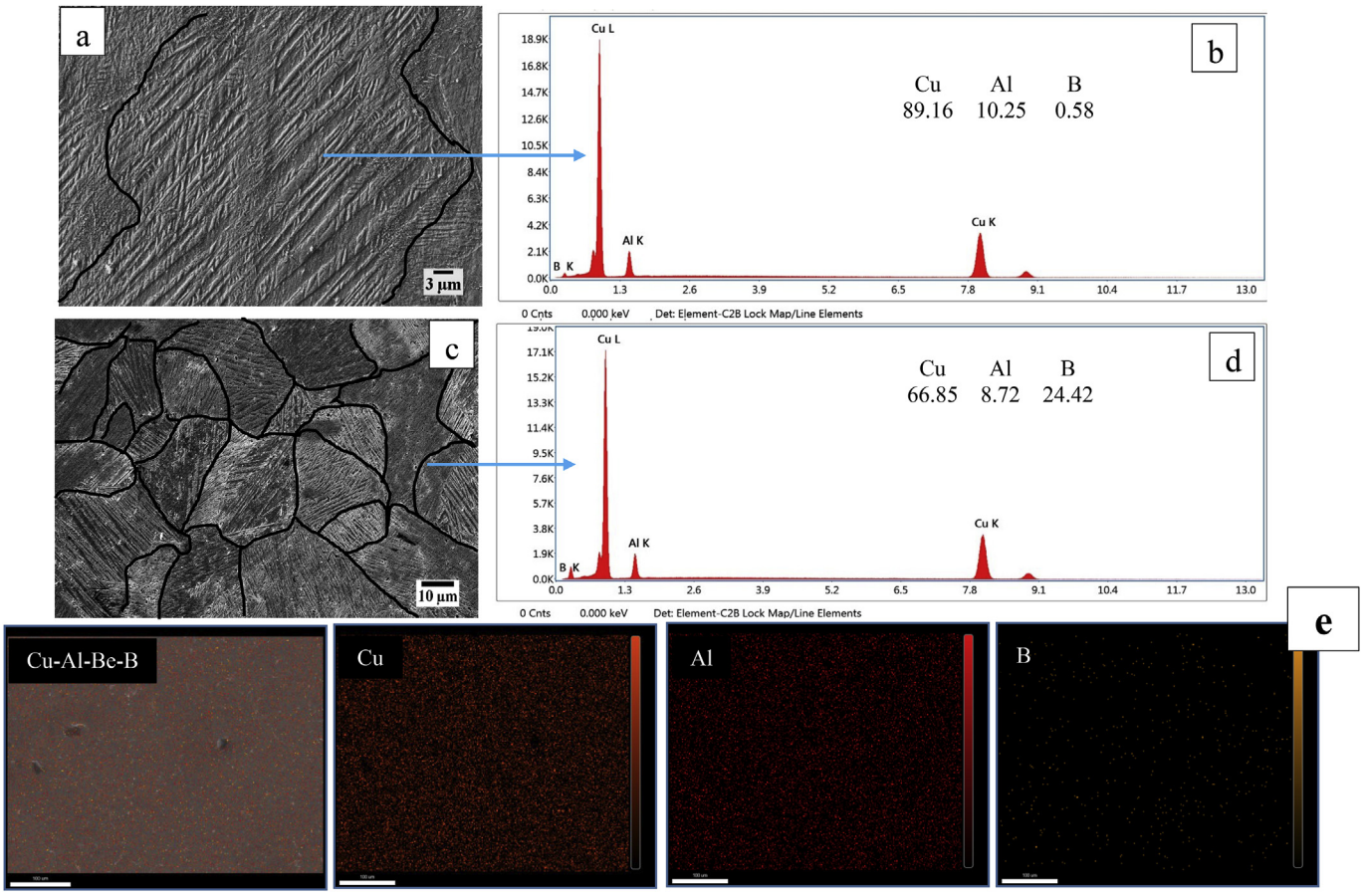

Fig. 10. SEM images; (a) B_{11} (c) B_{16}, EDS spectrum: (b) B_{11}, (d) B_{16}, Elemental mapping: (e) B_{16}.

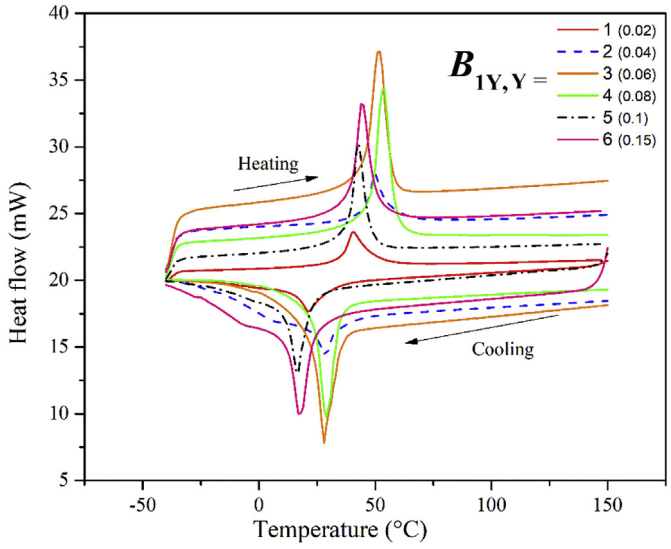

Fig. 11. Thermogram – B_{1Y} alloys.

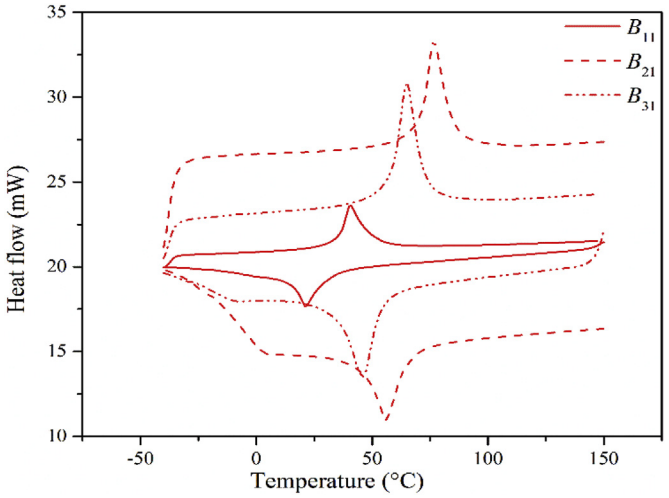

Fig. 12. Thermogram – B_{11}, B_{21} and B_{31} alloys.

The results are tabulated in Table 2 consists of tempeartures, enthalpies and hysteresis along with amount of differences in transformation tempeartures and hysteresis with the variation of wt.% of one element while keeping the remaining constant.

It is clearly understood from thermogram (Fig. 11), and Table 2., that increase in wt.% of B increases the transformation temperatures slightly and its enthalpies up to 0.08 wt%, confirmed with the rise and shift of curves ($B_{11} - B_{41}$) away from the ordinate, and above 0.08 wt% the transformation temperatures decreases can be seen with the fall and shift of curves towards ordinate. The variations in the transformation temperatures are due to variations in the elemental composition of the matrix and precipitates. Increase in transformation temperatures are due to the increase in concentration of insoluble particles i.e., B and AlB_2 particles in the

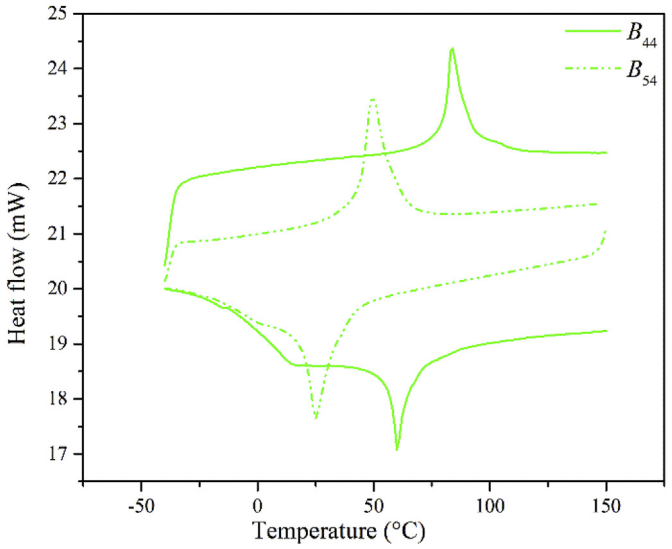

Fig. 13. Thermogram – B_{44}, B_{54} alloys.

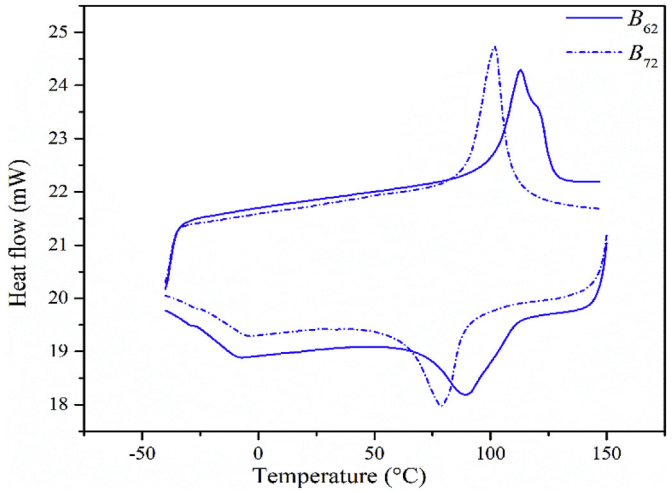

Fig. 14. Thermogram – B_{62}, B_{72} alloys.

matrix requires additional energy for phase transformation, and also increase in e/a ratio [31]. Increase in boron to 0.1 wt% and 0.15 wt% decreases transformation temperatures due to increased density of AlB_2 particles in the matrix depletes the Cu and Al, and increase B changes e/a ratio lowers the transformation tempeartures [8]. Increase in wt.% of B increases the thermal hysteresis irrespective of transformation tempeartures.

Thermogram $B_{21} - B_{31}$ and $B_{44} - B_{54}$ (Figs. 12 and 13) presents that only increase in addition of Al, decreases the transformation tempeartures [48] i.e., curves B_{21} falls to B_{31}, and B_{44} to B_{54}.shifts towards ordinate. Increase in 0.1 wt% of Al from B_{21} to B_{31} reduces M_f, M_s, A_s and A_f by 10, 11, 12, 11 °C almost ~11 °C, without a change in thermal hysteresis, whereas increase in 0.3 wt% of Al from reduces M_f, M_s, A_s and A_f by 7, 20, 12, 18 °C with 3 °C reduction in thermal hysteresis as shown in Table 2.

Thermogram B_{62}, B_{72} (Fig. 14) and B_{21}, B_{11} (Fig. 12) presents that only increase in Be, keeping other elements constant decreases the transformation temperatures. In the alloys B_{62} and B_{72}, increase in 0.1 wt% of Be reduces M_f, M_s, A_s and A_f by 36, 30, 36, 33 °C with slight increase in 2 °C of thermal hysteresis and shifts the curve towards ordinate, whereas in B_{21} and B_{11} alloys M_f, M_s, A_s and A_f reduces by 31, 35, 35, 35 °C, with fall and shift of curve towards ordinate.

3.4. Shape memory effect/shape recovery ratio

The shape recovery ratio of the alloys was calculated by the bend test as per the procedure discussed in section 2 and the results are presented in Fig. 15.

The results depicted in Fig. 15 conveys only B_{1X} series and B_{54} alloys yields 100% recovery and the rest exhibits poor recovery ratio. Complete recovery is due to complete formation of martensite $\beta_1' + \gamma'$ because of higher wt.% of Be and Al increases the martensite fraction. It is noticed that B_{21} and B_{31} yields 62.5% and 67.5% respectively, the poor recovery compared to the former alloys is due to addition of lower amount of Be i.e., 0.41 wt% forms partial α_2 phase along with martensite and are not suitable for memory applications, because of mixture of phases didn't exhibit shape recovery. but a slight increase in recovery i.e, 5% is noticed in B_{31} due to the 0.1% of increase in Al, increases martensite fraction. In the alloys B_{44} and B_{54}, it is understood that, though increase in addition of 0.45 wt% of Be, the poor recovery is due to the difference of 0.3 wt% of Al decreases the martensite fraction. B_{62} and B_{72} yields the lowest recovery ratio of the alloys i.e., 38% and 38.5% due to the

Table 2
Transformation temperatures (°C), Enthalpies (J/g) and Hysteresis (°C).

S. No	Alloy	M_f	M_s	$\Delta H_{A\rightarrow M}$	A_s	A_f	$\Delta H_{M\rightarrow A}$	Hysteresis ($A_f - M_s$)
1.	B_{11}	14	30	−6.2521	35	50	6.8865	20
2.	B_{12}	22	34	−7.9965	45	56	7.6268	22
3.	B_{13}	23	35	−16.5425	46	58	12.3201	23
4.	B_{14}	24	34	−25.4059	49	59	14.0765	25
5.	B_{15}	11	23	−11.7513	39	48	11.3864	25
6.	B_{16}	12	23	−9.2654	39	51	10.3261	28
7.	B_{21}	45	65	−7.2031	70	85	7.9448	20
8.	B_{31}	35	54	−9.4016	58	74	10.5234	20
	Diff	10	11	2.1985	12	11	2.5786	0
9.	B_{44}	56	64	−6.232	80	92	8.7203	28
10.	B_{54}	20	34	−5.8253	44	59	7.3070	25
	Diff	36	30	0.4067	36	33	1.4133	- 3
11.	B_{62}	69	108	−5.9189	101	127	7.3747	19
12.	B_{72}	62	88	−6.6619	89	109	9.3347	21
	Diff	7	20	0.743	12	18	1.96	+2
13.	B_{21}	45	65	−7.2031	70	85	7.9448	20
14.	B_{11}	14	30	−6.2521	35	50	6.8865	20
	Diff	31	35	0.951	35	35	1.0583	0

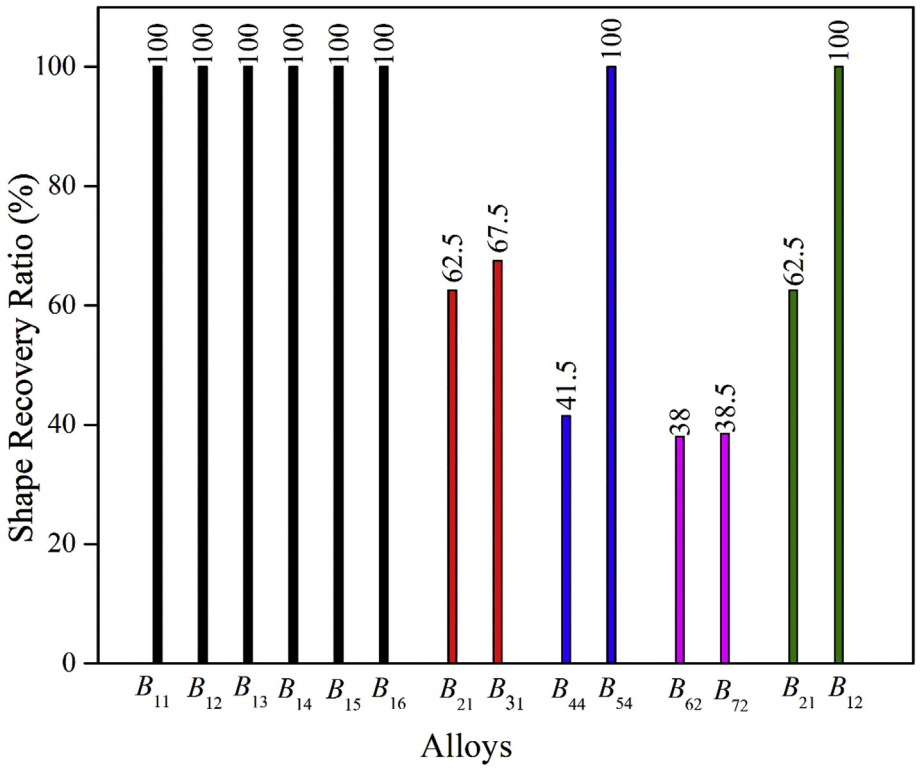

Fig. 15. Shape recovery ratio of alloys.

very low addition of Al i.e., 11.3 wt%, decreases the martensite fraction. B_{21} exhibits 100% recovery compared to B_{21} i.e., 62.5% due to lower addition of Be i.e., 0.41 wt% Be. From the shape recovery ratio studies, it is concluded that alloys more than 0.41 wt% of Be and 11.8 wt% Al exhibits rapid and complete shape recovery suitable for actuator applications.

4. Conclusions

Effect of microalloying of B and the variation of composition of Al and Be in the alloys has been investigated for the grain refinement and shape memory properties of polycrystalline Cu—Al—Be shape memory. Addition of B forms AlB_2 precipitates acts as nucleant and an effective grain refiner with minimal addition, due to the higher growth restriction factor and smaller lattice disregistry. Increase in B up to 0.08 wt% increases the transformation tempeartures and then decreases, whereas increase in both Al and Be decreases the transformation temperatures. Increase in addition of Al (>11.9 wt%) forms martensite of $\beta_1^{'} + \gamma^{'}$ variants and boron rich precipitates of $AlB_{25}Cu_{0.9}$. Addition of Be (<0.42 wt%) forms α_2 phase, not suitable for memory applications. Alloys with more than 0.41 wt% of Be and 11.8 wt% Al exhibits rapid and complete shape recovery suitable for actuator applications.

Declaration of competing interest

The authors declare that they have no known competing financial interests or personal relationships that could have appeared to influence the work reported in this paper.

CRediT authorship contribution statement

Guniputi Bala Narasimha: Conceptualization, Methodology, Investigation, Data curation, Formal analysis, Visualization, Writing - original draft. **S.M. Murigendrappa:** Writing - review & editing, Supervision, Validation, Funding acquisition, Project administration, Resources.

Acknowledgement

This study is financially supported by the SERB, Department of Science and Technology, Government of India, Project No: EMR/2016/001247.

References

[1] S. Miyazaki, K. Otsuka, H. Sakamoto, K. Shimizu, The fracture of Cu-Al-Ni shape memory alloy, Trans. Jpn. Inst. Met. 22 (1981) 244–252.
[2] R. Dasgupta, A.K. Jain, P. Kumar, S. Hussain, A. Pandey, Role of alloying additions on the properties of Cu-Al-Mn shape memory alloys, J. Alloy. Comp. 620 (2015) 60–66, https://doi.org/10.1016/j.jallcom.2014.09.047.
[3] C. Lopez del Castillo, M.L. Blazquez, C. Gomez, B.G. Mellor, N. de DIEGO, J. del RIO, The stabilization of martensite in Cu - Al - Mn alloys, J. Mater. Sci. 23 (1988) 3379–3382.
[4] D. Dunne, K. Ireland, C. Gonzalez, M. Morin, G. Guenin, Hyperstabilisation of martensite in Cu-Al-Be alloys, Mater. Sci. Eng. A 438–440 (2006) 339–342, https://doi.org/10.1016/j.msea.2006.02.139.
[5] J. Fernandez, A.V. Benedetti, J.M. Guilemany, X.M. Zhang, Thermal stability of the martensitic transformation of Cu – Al – Ni – Mn – Ti, Mater. Sci. Eng. A 440 (2006) 723–725, https://doi.org/10.1016/j.msea.2005.12.043.
[6] H. Flores Zuniga, D. Rios Jara, F.C. Lovey, G. Guenin, Thermal stability of beta phase in a Cu-Al-Be shape memory alloy, J. Phys. 1V. 5 (1995) 171–174.
[7] A.K. Jain, S. Hussain, P. Kumar, A. Pandey, D. Rupa, Effect of varying Al/Mn ratio on phase transformation in Cu – Al – Mn shape memory alloys, Trans. Indian Inst. Met. 69 (2016) 1289–1295, https://doi.org/10.1007/s12666-015-0689-3.
[8] X. Zhang, M. Zhang, T. Cui, J. Li, Q. Liu, H. Wang, The enhancement of the mechanical properties and the shape memory effect for the Cu-13 . 0Al-4 . 0Ni alloy by boron addition, J. Alloy. Comp. 776 (2019) 326–333, https://doi.org/10.1016/j.jallcom.2018.10.176.
[9] H. Sakamoto, K. Shimizu, Effect of heat treatments on thermally formed martensite phases in monocrystalline Cu-Al-Ni ShapeMemoryAlloy, ISIJ Int. 29 (1989) 395–404.
[10] S.N. Saud, E. Hamzah, T. Abubakar, S. Farahany, Structure-property relationship of Cu-Al-Ni-Fe shape memory alloys in different quenching media, J. Mater. Eng. Perform. 23 (2014) 255–261, https://doi.org/10.1007/s11665-

013-0759-9.
[11] M.M. Shafeeq, G.K. Gupta, M.M. Malik, V. Sampath, O.P. Modi, Influence of quenching methods on martensitic transformation and mechanical properties of P/M processed Cu–Al–Ni–Ti shape memory alloys, Powder Metall. 59 (2016) 271–280, https://doi.org/10.1080/00325899.2016.1206261.
[12] M. Izadinia, K. Dehghani, Structure and properties of nanostructured Cu-13.2Al-5.1Ni shape memory alloy produced by melt spinning, Trans. Nonferrous Metals Soc. China 21 (2011) 2037–2043, https://doi.org/10.1016/S1003-6326(11)60969-2.
[13] P. Zhang, A. Ma, S. Lu, P. Lin, J. Jiang, H. Ma, C. Chu, Effect of equal channel angular pressing and heat treatment on the microstructure of Cu-Al-Be-B shape memory alloy, Mater. Lett. 63 (2009) 2676–2679, https://doi.org/10.1016/j.matlet.2009.09.037.
[14] W.H. Zou, C.W.H. Lam, C.Y. Chung, J.K.L. Lai, Improvement of the shape memory characteristics of a Cu-Zn-Al alloy with manganese and zirconium addition, Scr. Mater. 36 (1997) 955–960, https://doi.org/10.1016/S1359-6462(96)00496-4.
[15] G. Bala Narasimha, S.M. Murigendrappa, Effect of zirconium on the properties of polycrystalline Cu-Al-Be shape memory alloy, Mater. Sci. Eng. A 755 (2019) 211–219, https://doi.org/10.1016/j.msea.2019.04.022.
[16] B.N. Guniputi, S.M. Murigendrappa, Influence of Gd on the microstructure, mechanical and shape memory properties of Cu-Al-Be polycrystalline shape memory alloy, Mater. Sci. Eng. A 737 (2018) 245–252, https://doi.org/10.1016/j.msea.2018.09.064.
[17] X. Lu, F. Chen, W. Li, Y. Zheng, Effect of Ce addition on the microstructure and damping properties of Cu-Al-Mn shape memory alloys, J. Alloy. Comp. 480 (2009) 608–611, https://doi.org/10.1016/j.jallcom.2009.01.134.
[18] J.W. Xu, Effects of Gd addition on microstructure and shape memory effect of Cu – Zn – Al alloy, J. Alloy. Comp. 448 (2008) 331–335, https://doi.org/10.1016/j.jallcom.2006.11.159.
[19] C. Aksu Canbay, A. Keskin, Effects of vanadium and cadmium on transformation temperatures of Cu-Al-Mn shape memory alloy, J. Therm. Anal. Calorim. 118 (2014) 1407–1412, https://doi.org/10.1007/s10973-014-4034-6.
[20] A.Y. Lozovoi, A.T. Paxton, Boron in copper: a perfect misfit in the bulk and cohesion enhancer at a grain boundary, Phys. Rev. B Condens. Matter Mater. Phys. 77 (2008) 1–16, https://doi.org/10.1103/PhysRevB.77.165413.
[21] M. Suresh, A. Srinivasan, K.R. Ravi, U.T.S. Pillai, B.C. Pai, Influence of boron addition on the grain refinement and mechanical properties of AZ91 Mg alloy, Mater. Sci. Eng. A 525 (2009) 207–210, https://doi.org/10.1016/j.msea.2009.07.019.
[22] T. Wang, Z. Chen, H. Fu, J. Xu, Y. Fu, T. Li, Grain refining potency of Al-B master alloy on pure aluminum, Scr. Mater. 64 (2011) 1121–1124, https://doi.org/10.1016/j.scriptamat.2011.03.001.
[23] Y. Birol, Grain refinement of Al–Cu foundry alloys with B additions, Int. J. Cast Met. Res. 25 (2012) 117–120, https://doi.org/10.1179/1743133611y.000000001155.
[24] M.J. Balart, J.B. Patel, F. Gao, Z. Fan, Grain refinement of deoxidized copper, Metall. Mater. Trans. A Phys. Metall. Mater. Sci. 47 (2016) 4988–5011, https://doi.org/10.1007/s11661-016-3671-8.
[25] J.R. Davis, A.S.M.I.H. Committee, Copper and Copper Alloys, ASM International, 2001. https://books.google.co.in/books?id=sxkPJzmkhnUC.
[26] J.S. Lee, C.M. Wayman, Grain refinement of Cu-Zn-AI shape memory alloys, Metallography 19 (1986) 401–419.
[27] Y.Y. Dong, T.M. Wang, S.J. Zin, K.Z. Dar, The shape memory capability and life of Cu-Al-Be-X alloys, Mater. Char. 33 (1994) 163–168, https://doi.org/10.1016/1044-5803(94)90079-5.
[28] Y.Y. Dong, C.M. Wang, Y.P. Gu, Y.G. Liu, Phenomena of aluminum segregation at the grain boundaries of CuAlBe-X alloys, Mater. Sci. Forum 394–395 (2002) 209–212. https://doi.org/10.4028/www.scientific.net/MSF.394-395.209.
[29] V. Sampath, U.S. Mallik, Influence of minor additions of boron and zirconium on shape memory properties and grain refinement of a Cu-Al-Mn shape memory alloy, Mater. Soc. Annu. Meet. (2009) 181–188, https://doi.org/10.1051/esomat/200905028, 05028.
[30] U.S. Mallik, V. Sampath, Effect of grain refinement on shape memory properties of Cu-Al-Mn SMAs, Adv. Mater. Res. 1101 (2015) 104–107. https://doi.org/10.4028/www.scientific.net/AMR.1101.104.
[31] Y.A.A.S. Turabi, A.A.E.D. Vance, The effects of substituting B for Cu on the magnetic and shape memory properties of CuAlMnB alloys, Appl. Phys. A 122 (2016) 1–8, https://doi.org/10.1007/s00339-016-0222-5.
[32] V. Sampath, Improvement of shape-memory characteristics and mechanical properties of copper-zinc-aluminum shape-memory alloy with low aluminum content by grain refinement, Mater. Manuf. Process. 21 (2006) 789–795, https://doi.org/10.1080/10426910600837756.
[33] Y. Sutou, T. Omori, N. Koeda, R. Kainuma, K. Ishida, Effects of grain size and texture on damping properties of Cu-Al-Mn-based shape memory alloys, Mater. Sci. Eng. A 438–440 (2006) 743–746, https://doi.org/10.1016/j.msea.2006.02.085.
[34] N. Koeda, T. Omori, Y. Sutou, H. Suzuki, M. Wakita, R. Kainuma, K. Ishida, Damping properties of ductile Cu-Al-Mn-based shape memory, Alloys 46 (2005) 198–201.
[35] K. Noriyuki, O. Isao, T. Yoshitsugu, E. Tetsuo, Formation process of α2 phase in Cu-Al alloys, Trans. Jpn. Inst. Met. 18 (1977) 195–203.
[36] H. Warlimontt, The electron-metallography and crystallography of copper-alumnium martensites, Acta Metall. 11 (1963) 511–527.
[37] M.A. Morris, High temperature properties of ductile Cu-Al-Ni shape memory alloys with boron additions, Acta Met. Mater. 40 (1992) 1573–1586.
[38] S. Hussain, A. Pandey, R. Dasgupta, Designed polycrystalline ultra-high ductile boron doped Cu–Al–Ni based shape memory alloy, Mater. Lett. 240 (2019) 157–160, https://doi.org/10.1016/j.matlet.2018.12.142.
[39] H. Baker, H. Okamoto, ASM Handbook. Vol. 3. Alloy Phase Diagrams, ASM International, Materials Park, Ohio 44073-0002, USA, 1992, 501, 1992.
[40] X. Wang, The formation of AlB2 in an Al-B master alloy, J. Alloy. Comp. 403 (2005) 283–287, https://doi.org/10.1016/j.jallcom.2005.04.204.
[41] H. Duschanek, P. Rogl, The Al-B (Aluminum-Boron) system, J. Phase Equilibria 15 (1994) 543–552.
[42] Z. Chen, H. Kang, G. Fan, J. Li, Y. Lu, J. Jie, Y. Zhang, T. Li, X. Jian, T. Wang, Grain refinement of hypoeutectic Al-Si alloys with B, Acta Mater. 120 (2016) 168–178, https://doi.org/10.1016/j.actamat.2016.08.045.
[43] H.U. Hong, H.W. Jeong, I.S. Kim, B.G. Choi, Y.S. Yoo, C.Y. Jo, Significant decrease in interfacial energy of grain boundary through serrated grain boundary transition, Philos. Mag. 6435 (2012), https://doi.org/10.1080/14786435.2012.676212.
[44] A.K. Koul, R. Thamburaj, Serrated grain boundary formation potential of Ni-based superalloys and its implications, Metall. Trans. A. 16 (1985) 17–26.
[45] P. Emadi, Grain Refinement of Magnesium and AZ91E Magnesium Alloy by Addition of MgB2 Inoculant, Ryerson University, 2014. https://digital.library.ryerson.ca/islandora/object/RULA%3A7669.
[46] M. Zhu, X. Ye, C. Li, G. Song, Q. Zhai, Preparation of single crystal CuAlNiBe SMA and its performances, J. Alloy. Comp. 478 (2009) 404–410, https://doi.org/10.1016/j.jallcom.2008.11.051.
[47] S. Ergen, O. Uzun, F. Yilmaz, M.F. Kiliçaslan, Shape memory properties and microstructural evolution of rapidly solidified CuAlBe alloys, Mater. Char. 80 (2013) 92–97, https://doi.org/10.1016/j.matchar.2013.03.010.
[48] A. Higuchi, K. Suzuki, Y. Matsumoto, K. Sugimoto, S. Komatsu, Y. Nakamura, Shape memory effect in Cu-Al-Be ternary alloys, J. Phys. Colloq. 43 (1982) C4–C767.